Organic & Biomolecular Chemistry

PAPER

View Article Online
View Journal | View Issue

Cite this: *Org. Biomol. Chem.*, 2015, **13**, 7681

Highly water-soluble and tumor-targeted photosensitizers for photodynamic therapy†

Yuxi Li,‡[a,b] Jin Wang,‡[b] Xiaoxiao Zhang,[b] Wenjun Guo,[b] Fu Li,[a] Min Yu,[b] Xiuqi Kong,[b] Wenjie Wu*[a] and Zhangyong Hong*[b]

Received 22nd May 2015,
Accepted 4th June 2015

DOI: 10.1039/c5ob01035g

www.rsc.org/obc

Biological uses of photosensitizers in photodynamic therapy (PDT) often suffer from a lack of tumor selectivity; a strategy based on molecule-targeted cancer therapies could provide a promising solution. To synthesize new water-soluble phthalocyanines (Pcs) for bio-conjugation with peptides or antibodies, we developed a method to synthesize asymmetrically substituted Pcs with both high water solubility and one monoamino group for conjugation with biological agents for tumor homing, using folic acid as the ligand model to direct the modified Pcs into target cells. Here, we report studies on the syntheses and characterization of these Pcs. *In vitro* and *in vivo* assays prove that the high solubility characteristic can greatly increase the tumor targeting capability of Pcs by reducing non-specific uptake. This newly designed photosensitizer accumulated almost completely in tumor regions, with a negligible signal found in other tissues in the xenograft tumor model. These initial data provide strong evidence of the high specificity tumor targeting of Pcs with folate and tri-glycerol substitutions. Theoretically, the synthesized Pcs could be conveniently conjugated to many other ligands, endorsing the broad applicability of this method for tumor-targeted PDT.

1. Introduction

Photodynamic therapy (PDT) is a therapeutic procedure utilizing a photosensitizer activated by light to create irreversible photo-damage to tissues, which has become a well-established therapeutic modality for the treatment of a variety of premalignant and malignant diseases.[1] As a non-invasive modality, PDT combines three individually harmless components, a photosensitizer, light, and molecular oxygen, to generate reactive oxygen species (ROS) leading to cellular and tissue damage.[2] PDT also has the advantages of repeated dose tolerance and high specificity, which are achieved through the precise application of light.[3] Furthermore, PDT agents act as fluorescent probes to be used for fluorescence imaging technology, which could offer superior sensitivity and real-time imaging for *in vivo* cancer diagnoses and presentations.[4] Clearly identifying cancer cells before or during treatment would likely increase the success of therapy. The natural connection of near-infrared (NIR) fluorescence imaging with photodynamic therapy (PDT) forms a beneficial union for application as a noninvasive tool for cancer therapy.[5]

The synthesis of photosensitizers with desired properties is considered to be an important bottleneck in PDT therapy.[6] Ideal photosensitizers are non-toxic to the host in the absence of light, accumulate preferentially in tumor tissue, and most importantly, have a high molar absorption coefficient and high singlet oxygen generation efficiency in the biological wavelength window (650–900 nm) for deeper penetration into biological tissues.[7] Traditionally, porphyrin-based photosensitizers have dominated the PDT field, and they usually have a relatively weak satellite absorption band (Q-band) in the region of 600–650 nm.[8] Phthalocyanines (Pcs), as next generation photosensitizers, are among the most promising candidates for PDT and have received considerable attention.[9] They offer multiple desirable characteristics, such as strong light absorption at long wavelengths (650 nm to 850 nm), high efficiency of singlet oxygen generation, extraordinary stability and biocompatibility.[10] Furthermore, the spectral and photophysical properties of Pcs can be easily tuned by varying the substituents around the Pc aromatic core or the central metal.[11]

For most Pcs, extremely low solubility and aggregation phenomena in water render them photodynamically inactive in aqueous medium and thus significantly restrict their *in vivo* biological and medical applications.[12] Pcs have not been syste-

[a]*College of Material Science and Chemical Engineering, Tianjin University of Science and Technology, Tianjin 300457, P. R. China. E-mail: wwjie@tust.edu.cn; Tel: +86 022 23502875*

[b]*State Key Laboratory of Medicinal Chemical Biology, College of Life Sciences, Nankai University, Tianjin 300071, P. R. China. E-mail: hongzy@nankai.edu.cn; Tel: +86 022 23498707*

†Electronic supplementary information (ESI) available: Synthetic procedure for resin-bound phthalonitrile, HPLC chromatogram, ESI-HRMS and NMR data of the phthalocyanines. See DOI: 10.1039/c5ob01035g

‡Yuxi Li and Jin Wang contributed equally to this work.

matically studied in aqueous solutions. In the literature, detailed attention has been given to the absorption and emission properties of Pcs in DMSO solutions, in which extremely low solubility could be obtained.[13] To become promising photosensitizers, high singlet oxygen quantum yields in aqueous medium are necessary, thus water-solubility represents an important characteristic of good photosensitizers.

Many studies have focused on the optimization of Pcs to use Pcs in aqueous media.[11,14] A historical approach was to incorporate insoluble Pcs primarily in liposomes, biodegradable polymeric nanoparticles, or emulsions with the use of a surfactant, *e.g.*, Cremophor EL.[15] Other efficient strategies include chemical modification of Pcs through the attachment of appropriate hydrophilic substituents. Until recently, most of the chemical modifications have been performed based on the attachment of ionic substituents, such as sulfonates[16] and carboxylates[17] to form anionic Pcs, or quaternized amino[18] and aromatic groups[19] to form cationic Pcs. Ionic substitutions can strongly affect the characteristics of Pcs, leading to increased water solubility and a reduced degree of aggregation as well as a high rate of singlet oxygen generation. However, they also have serious drawbacks, including interaction with the constituents of biological fluids (*e.g.*, plasma proteins) and interfaces[20] (*e.g.*, cell membrane) and causing serious side effects. Non-ionic water-soluble Pcs represent another efficient way to solve the solubility problems of Pcs, although studies of their synthesis and application are rare. Recently several non-ionic water-soluble Pcs have been synthesized through modification with functional groups, such as carbohydrate substitution and polyhydroxylate substitution.[21]

Conventional PDT for cancer therapy is based on the preferential accumulation of a photosensitizer in tumors with minimal damage to normal tissues. However, because the existing photosensitizers lack tumor selectivity, considerable damage occurs in normal tissues, which leads to unwanted toxicity. Thus, current methods of PDT would be improved if more selective targeting of the photosensitizer was possible, which would increase the uptake of PDT agents by the targeted cancer cells. Most attempts at targeting have been performed through encapsulation in liposomes and polymeric nanoparticles *via* an enhanced permeability and retention (EPR) effect of tumor accumulation.[22] Conjugation with various tumor-specific vehicles, such as epidermal growth factor, monoclonal antibodies[23] and small molecule ligands (*e.g.*, short peptides or peptidomimetics) would provide another promising strategy to increase the selectivity of photosensitizers with precise targeting properties. However, most of the synthesized Pcs are not suitable for use in bio-conjugation, as unique functional groups on the structure of Pcs that are needed for attachment are missing. The asymmetrically substituted A_3B-type Pcs with one reactive group for conjugation are ideally suited for these applications,[24] but difficulties in the synthesis and isolation of these Pcs have limited their application.[25] Recently reported solid-phase synthesis of Pcs presents an efficient method for the synthesis of pure AB_3-type mono-functionalized Pcs.[26]

For the above reasons, new types of Pcs with high water solubility, as well as with one or more functional groups for conjugation with biological agents, have been anxiously awaited. Here, we report our study on the synthesis and characterization of only such an asymmetrically substituted highly water-soluble Pc with two different types of peripheral substituents: one reactive group for conjugation and others for solubility. The functionalized amine group can be conveniently conjugated with ligands, herein with folic acid as a model, for tumor targeting purposes.[27] The high solubility characteristic can greatly reduce non-specific uptake and thus reduce the background. However, the tumor homing ligand can selectively bring the PDT agents inside tumor cells. The evaluation of their photophysical and photochemical properties both *in vitro* and *in vivo* proves that they have high potential as tumor-selective PDT agents. These preliminary studies may offer a useful strategy in the quest for more efficient tumor-selective Pcs for PDT.

2. Results and discussion

2.1. Molecular design of water-soluble Pcs

Biological uses of photosensitizers in PDT often suffer from a lack of tumor selectivity. Taking advantage of highly specific receptor–ligand interactions to direct the photosensitizers into target cells leads to efficient strategies to solve this problem. To synthesize new water-soluble Pcs for bio-conjugation with peptides or antibodies, asymmetrically substituted Pcs with two different types of peripheral substituents, one reactive group for conjugation and others for solubility, were designed (Fig. 1, $PcZn_1$-lys and $PcZn_2$-lys). For conjugation, an asymmetric monoamino group was added using the strategy of solid phase synthesis of un-symmetric AB_3 type Pcs. Folic acid was selected to covalently conjugate to these asymmetrically substituted Pcs as model tumor-homing ligands for tumor targeting purposes (Fig. 1, $PcZn_1$-lys-FA and $PcZn_2$-lys-FA). For comparison, two types of hydrophilic substitutions, a triethylene glycol monomethyl ether group and a glycerol group, were adopted to increase solubility and reduce aggregation by attachment to peripheral positions of the macrocycle. The symmetrical tetra-substituted $PcZn_1$ and $PcZn_2$ were also synthesized for comparison. The water solubility and photochemistry of these Pcs were tested and compared. Theoretically, the synthesized Pcs could be conveniently conjugated to many other ligands for targeted PDT.

2.2. Synthesis of symmetric tetra-substituted Pcs

Scheme 1 shows the synthesis route used to prepare the tetra-substituted $PcZn_1$ and $PcZn_2$. 4-Nitrophthalonitrile reacts with triethyleneglycol monomethylether **8** and *S*-(+)-2,2-dimethyl-1,3-dioxolane-4-methanol **10**, leading, respectively, to monosubstituted phthalonitriles **9** and **11** in a 74% yield and 71% yield. These monosubstituted phthalonitriles were cyclotetramerized into $PcZn_1$ and isopropylidene protected Pc **11** in the presence of $Zn(OAc)_2{\cdot}2H_2O$ and 1,8-diazabicyclo[5.4.0]undec-7-

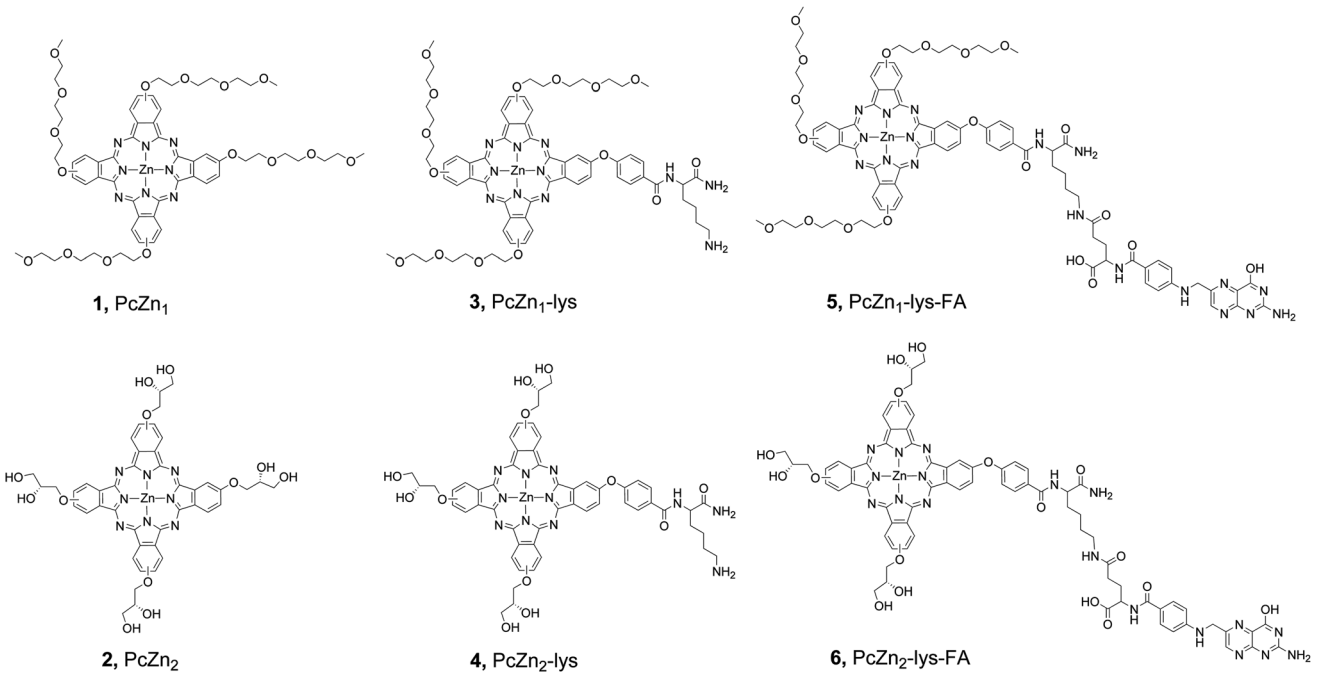

Fig. 1 The structure of the designed Pcs.

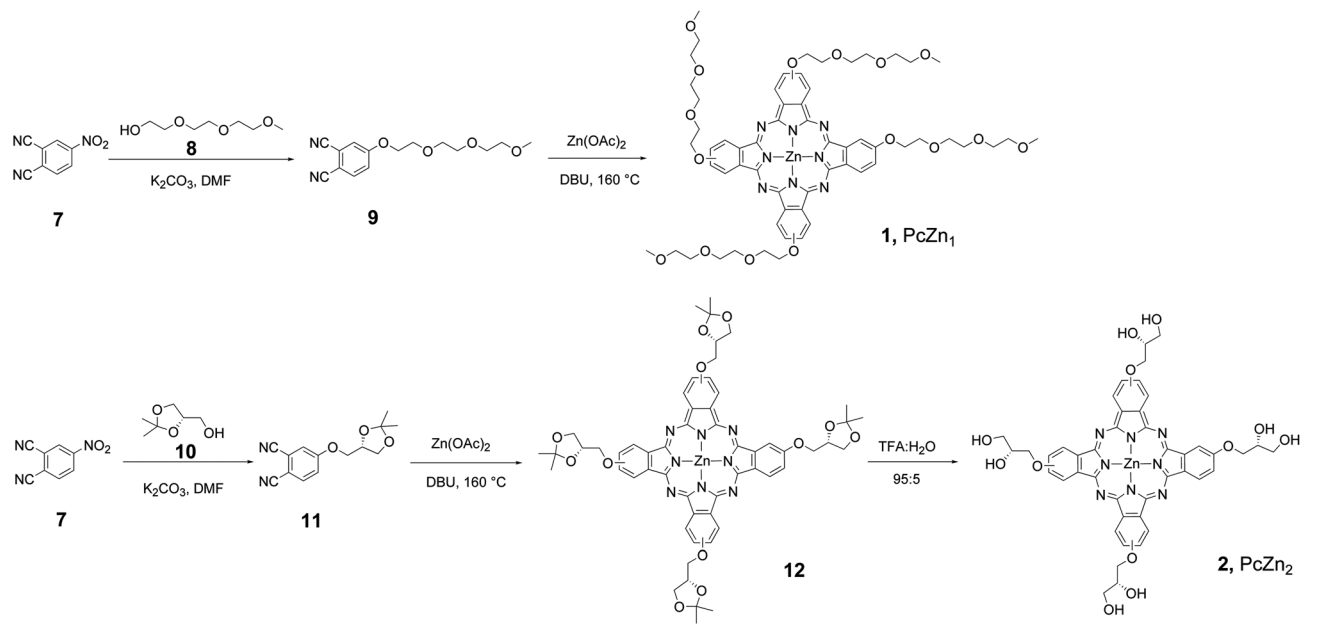

Scheme 1 The syntheses of the symmetric Pcs with hydrophilic moiety substitutions.

ene (DBU) in *n*-hexyl alcohol. The isopropylidene group of **12** could be removed readily upon treatment with a mixture of trifluoroacetic acid (TFA) and H_2O (9 : 1 v/v), generating $PcZn_2$ in 93% yield. The prepared $PcZn_1$ and $PcZn_2$ can be easily dissolved in water. These oxygen-rich substituents added to the peripheral positions of the macrocycles can greatly enhance the solubility of $PcZn_1$ and $PcZn_2$ in water. However, glycerol substitution has stronger effects; glycerol substituted $PcZn_2$ has an even higher water solubility than the respective triethyleneglycol monomethylether substituted $PcZn_1$. The structures of the new compounds were confirmed by NMR and high resolution mass spectrometry (HRMS). The ^1H NMR spectra of $PcZn_1$ and $PcZn_2$ show that the Pc protons appear at a lower field as a set of three multiplets, two multiplets between d 8.5

and 9.1 ppm due to the resonances of the eight Pc-alpha protons and a multiplet at d 7.6 and 7.8 ppm due to the four Pc-beta protons. The ESI-HRMS mass spectrum of $PcZn_1$ and $PcZn_2$ displayed ion peaks at m/z = 1247.4251 $[M + Na]^+$ and 937.2102 $[M + H]^+$, respectively, which confirmed the proposed structures.

2.3. Synthesis of asymmetric tetra-substituted Pcs using solid-phase synthesis

Solid-phase synthesis was utilized for the preparation of asymmetric highly water-soluble AB_3-type $PcZn_1$-lys and $PcZn_2$-lys with monoamino substitution (as shown in Scheme 2) for the convenient purification of the isotypes. The syntheses started from an amine-functionalized, solid-supported phthalonitrile **13** (see the ESI† for the synthesis of **13**). Briefly, a suspension of polymer-bound phthalonitrile **13**, triethyleneglycol monomethylether-substituted phthalonitrile **9** or glycerol-substituted phthalonitrile **11**, $Zn(OAc)_2$, and DBU in *n*-hexyl alcohol were heated to 160 °C for 5 h to generate polymer-bound AB_3-type Pc. The resin was washed with methanol and CH_2Cl_2 until a colorless filtrate was collected, cleaved in 95% TFA with triisopropylsilane (TIS) (TFA : H_2O : TIS = 95 : 2.5 : 2.5), and was then precipitated with diethyl ether and purified with HPLC to afford AB_3-type asymmetrical $PcZn_1$-lys in approximately 20–30% yield. In addition to the resin, the 4-methyltrityl (Mtt) group was also cleaved through TFA treatment. $PcZn_2$-lys with glycerol-substituted chains was synthesized similarly, but the cutting reagent was changed to a solution of TFA/H_2O (95 : 5) without TIS, as TIS could interfere with the isopropylidene group and result in a very complex product. Synthesis of $ZnPc_1$-lys and $PcZn_2$-lys supports the applicability of this method to many other types of asymmetric Pcs.

2.4. Conjugate of folic acid with the asymmetric tetra-substituted Pcs

The synthesized asymmetric $PcZn_1$-lys and $PcZn_2$-lys could be conveniently conjugated to biomolecules, such as antibodies, proteins or peptide ligands for selective tumor targeting purposes in PDT. To test the application potential of these asymmetric Pcs, we selected folic acid as the tumor homing ligand to synthesize asymmetrically substituted $PcZn_1$-lys-FA and $PcZn_2$-lys-FA. Two coupling strategies were tested for this purpose. In the first (Scheme 3), the coupling reaction was conducted on the solid support. The Mtt group was selectively removed by treatment with a 2% trifluoroacetic acid solution (TFA : DCM : TIS = 2 : 96 : 2) without cleaving the Pc from the solid support. Then, folate was coupled in the presence of HBTU and DIEA in a solution of DMF/DMSO (1 : 1). Finally, polymer-bound AB_3-type Pc was treated with 95% TFA (TFA : H_2O = 95 : 5) to yield the desired $PcZn_1$-lys-FA or $PcZn_2$-lys-FA. In the second strategy (Scheme 4), the coupling of folate was performed directly in the solution phase by the reaction of $PcZn_1$-lys or $PcZn_2$-lys with NHS-activated folate in DMSO solution, and the product was precipitated with diethyl ether and purified through HPLC to produce $PcZn_1$-lys-FA in 75% yield or $PcZn_2$-lys-FA in 80% yield.

2.5. Ground state electron absorption and aggregation behavior

The electronic spectra of the synthesized Pcs consist of an intense and sharp absorption band (Q band) at 682 nm and a broad Soret band (B band) at approximately 350 nm in DMSO (Table 1 and Fig. 2), which are characteristic absorptions of Pcs. Compared with the non-substituted ZnPc (~670 nm, as shown in the ESI†), the Q band area is red-shifted during its

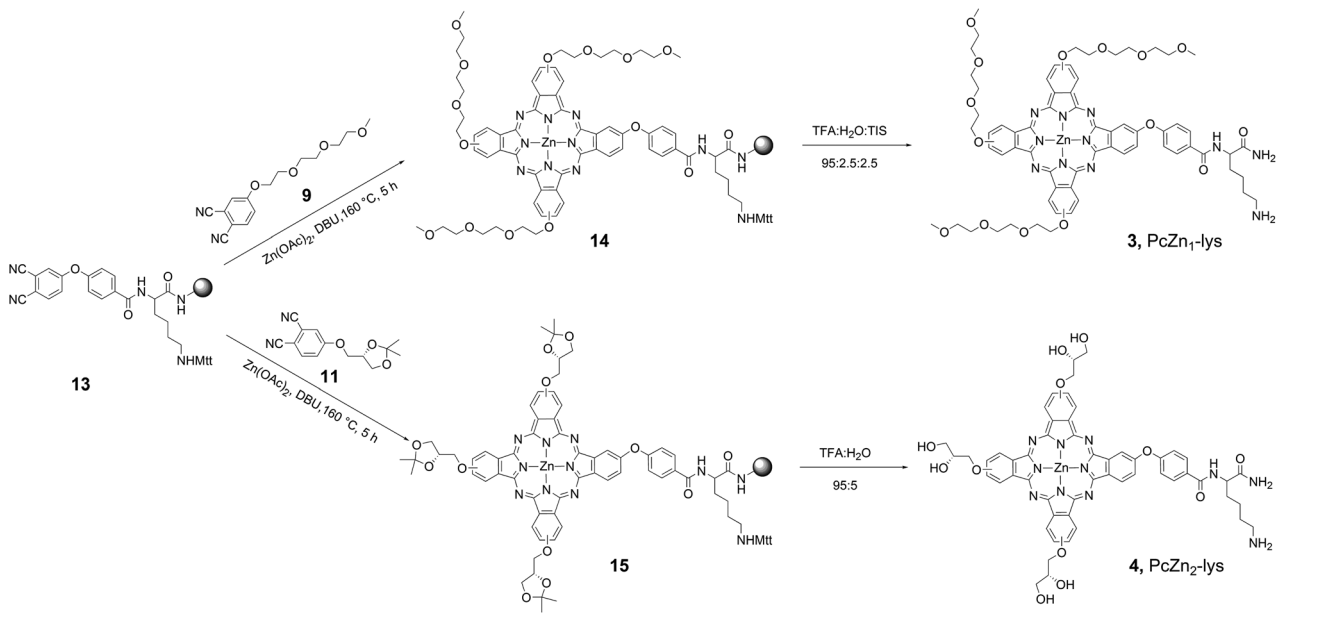

Scheme 2 Solid-phase syntheses of the asymmetric Pcs with monoamino group and hydrophilic moiety substitutions.

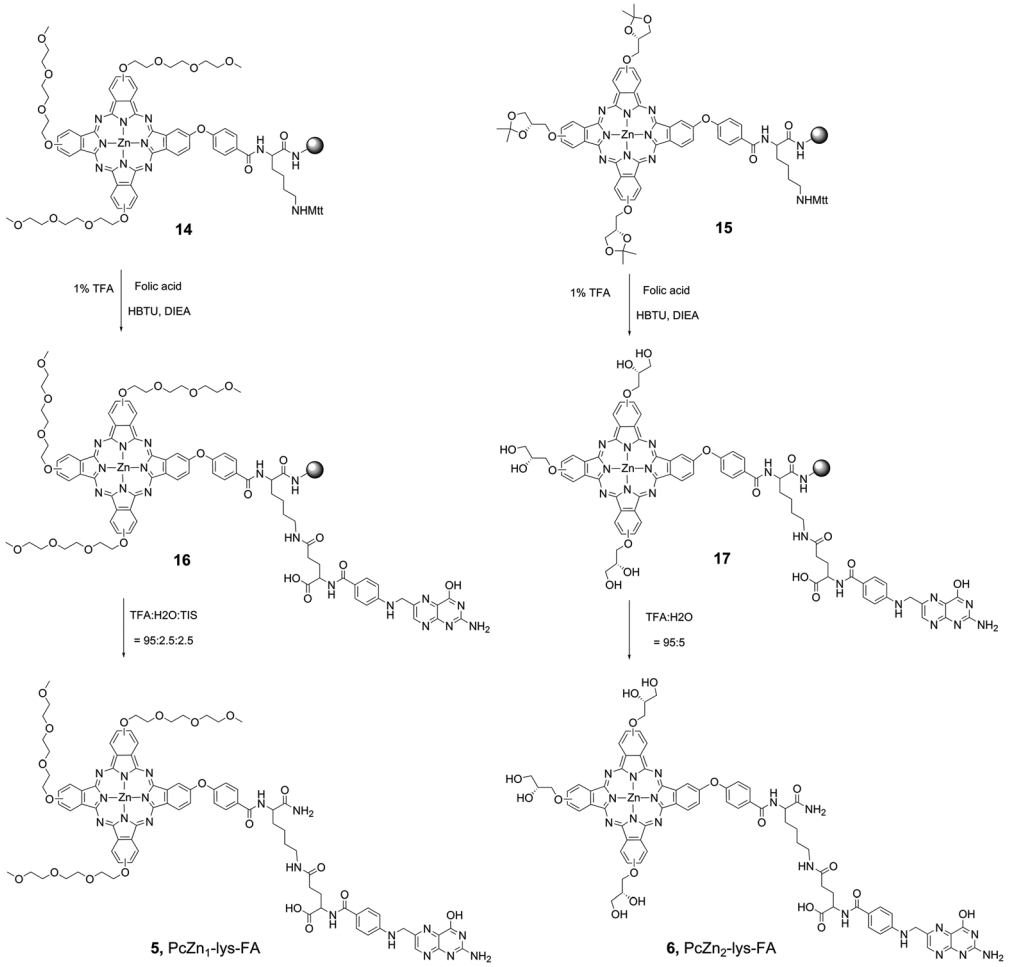

Scheme 3 The conjugation of folate with the water soluble asymmetric Pcs on resin.

peripheral substitution, as can been explained by the attachment of the electron-donating alkoxy groups at the peripheral positions, reducing the energy gap of the Highest Occupied Molecular Orbital (HOMO)–Lowest Unoccupied Molecular Orbital (LUMO) of the Pc ring.

Pcs are notorious for their strong tendency to aggregate, which can significantly decrease their photosensitizing ability through self-quenching. Hydrophilic substitutions can reduce the aggregation tendency of the Pc core. The UV–Vis spectra of the Pcs were highly sensitive to the aggregation characteristics, which can be used to indicate the aggregation status. The electronic spectra of all six of the synthesized Pcs in DMSO showed completely monomeric behavior, as evidenced by a single and narrow Q band (Fig. 2), typical for non-aggregated Pcs. However, in the spectra of the un-substituted ZnPc (shown in the ESI, Fig. S5†), in addition to intense Q absorption bands at 670 nm, weaker absorptions at 621 nm were also present, which are generally observed in the presence of aggregated species. The aggregation behavior of the Pcs in DMSO were also investigated through the analysis of the concentration dependence of their UV–Vis spectra in concentrations ranging from 1.0×10^{-5} to 2.0×10^{-6} M, as aggregation is always concentration dependent (Fig. 2). The spectra had no new bands appearing (normally blue-shifted) because the aggregated species and the normalized spectra at all concentrations could be superimposed without a change in the shape of the Q-band. The intensity of the absorption of the Q band increased with the increase in concentration, obeying the Beer–Lambert law, which suggested that aggregation of these compounds in DMSO is negligible.

DMSO is known to be able to greatly reduce aggregation because it binds axially to zinc(II) Pcs as a coordinating solvent. However, the electronic spectra of the formed Pcs in water showed differences (Fig. 3), although all of these Pcs are soluble in water. Their absorption spectra suggest cofacial aggregation in water, as evidenced by the presence of a higher energy (blue-shifted) band at 620–640 nm in the Q band region. This is evidence of the fact that both types of hydrophilic substitutions cannot completely solve the aggregation problems of Pcs in water, even though all of the synthesized Pcs have high water solubility. However, complete de-aggregation of Pcs in pure water solution may not be necessary, as the

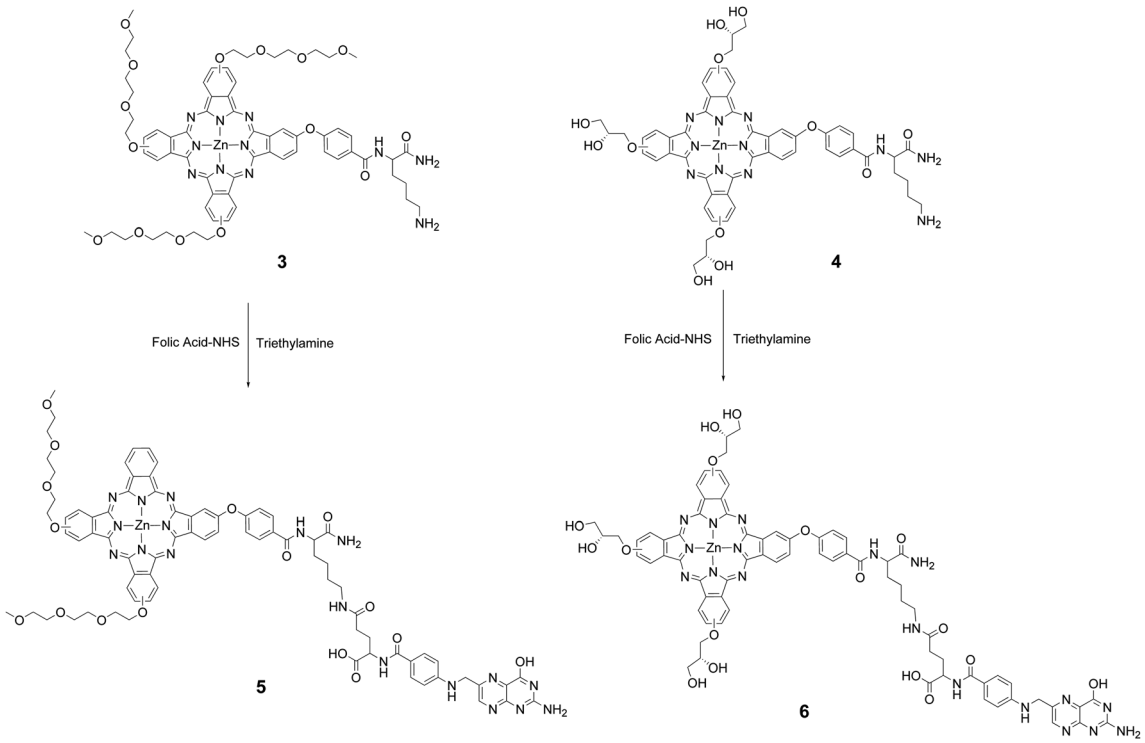

Scheme 4 The conjugation of folate with the water soluble asymmetric Pcs in solution.

Table 1 Absorption spectral data of $PcZn_1$, $PcZn_1$-lys, $PcZn_1$-lys-FA, $PcZn_2$, $PcZn_2$-lys and $PcZn_2$-lys-FA in DMSO, H_2O and a H_2O + Triton X-100 solution. For ZnPcs in DMSO, λ_{max} = 672 nm, log ε = 5.14

Compound	Solvent	λ_{max}/nm (log ε)
$PcZn_1$	DMSO	682 (4.85)
	H_2O	629, 689
	H_2O + Triton X-100	616, 684
$PcZn_1$-lys	DMSO	682 (4.73)
	H_2O	631, 677
	H_2O + Triton X-100	614, 682
$PcZn_1$-lys-FA	DMSO	682 (4.89)
	H_2O	641, 687
	H_2O + Triton X-100	—, 685
$PcZn_2$	DMSO	683 (4.69)
	H_2O	627, —
	H_2O + Triton X-100	617,685
$PcZn_2$-lys	DMSO	682 (4.65)
	H_2O	630, —
	H_2O + Triton X-100	615, 684
$PcZn_2$-lys-FA	DMSO	682 (4.70)
	H_2O	630, —
	H_2O + Triton X-100	614, 683

pure water solution cannot completely mimic physiological conditions and PDT agents could be de-aggregated to recover their functions once they form complexes with lipids, the important constituents of the cell membrane or organelle membranes. Recently Makoto Mitsunaga found that photosensitizers can be effectively activated to kill tumor cells through adhesion to the cell membrane.[23a] Therefore, Triton X-100 was added to the water solution of the six substituted Pcs (concentration = 0.5×10^{-5} M) to mimic the lipid environment of cell membranes, and its ability to de-aggregate Pcs was determined. The results (Fig. 3) showed that the aggregation of these molecules can be broken up in the presence of Triton X-100 (10%). It is interesting to note the difference between $PcZn_1$-lys-FA and $PcZn_2$-lys-FA compounds. The addition of Triton X-100 can only partially break up the aggregation of $PcZn_1$-lys-FA (Fig. 3C), yet it completely broke up $PcZn_2$-lys-FA (Fig. 3F) aggregates, indicating that a glycol chain substitution on Pcs has a stronger capability to decrease the aggregation tendency of Pcs in aqueous media compared to triethyleneglycol monomethylether substitution. Alternatively, FA conjugation may reduce the water solubility and then increase the aggregation of these conjugates.

2.6. Fluorescence spectroscopy

The fluorescence excitation and emission spectra of all Pcs were determined in DMSO, as shown in Fig. 4. All of the synthesized Pcs display a fluorescent excitation band at approximately 684 nm and an emission band at approximately 694 nm in DMSO. They all showed similar fluorescence behavior, and the shape of their excitation spectra was similar to that of the absorption spectra.

Although these Pcs have a quite low fluorescence intensity in water, the addition of Triton X-100 to the water solutions of these Pcs can greatly increase the intensity of these complexes

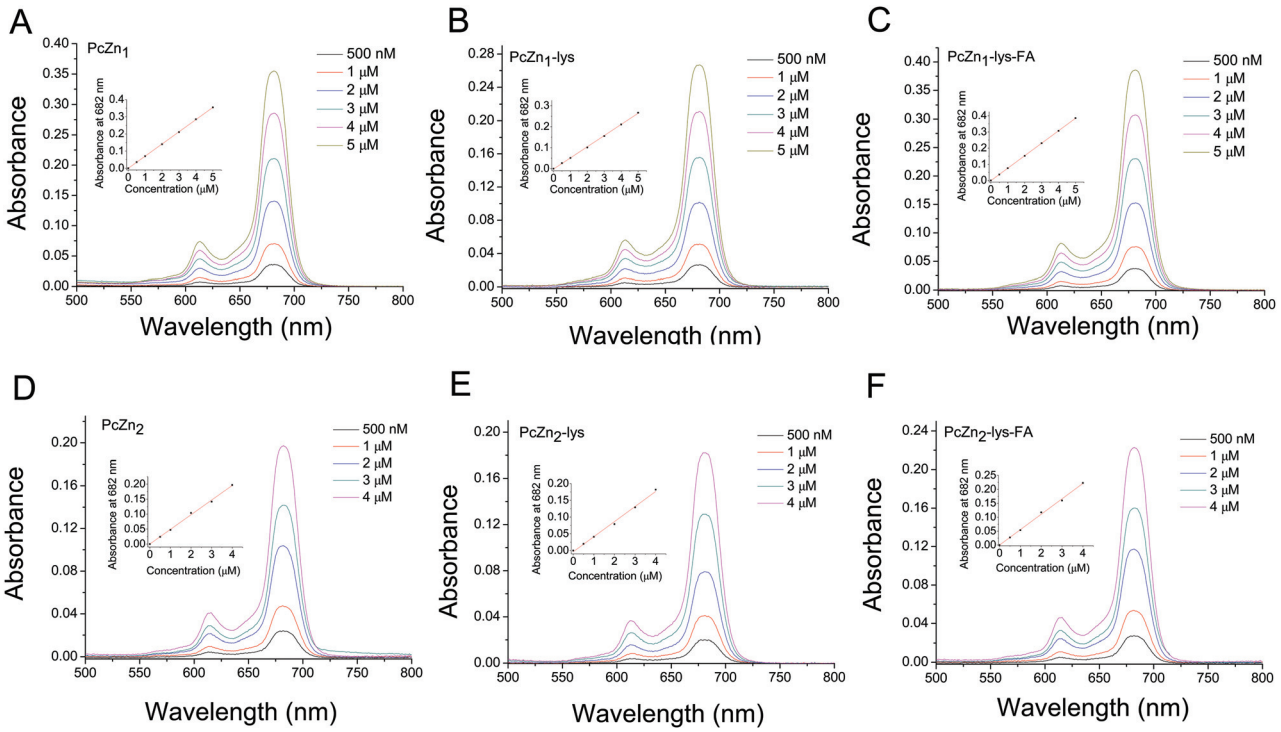

Fig. 2 Absorption spectra of $PcZn_1$ (a), $PcZn_1$-lys (b), $PcZn_1$-lys-FA (c), $PcZn_2$ (d), $PcZn_2$-lys (e) and $PcZn_2$-lys-FA (f) at various concentrations in DMSO. The inset plots are Q-band absorbance *versus* the concentration of the corresponding compounds.

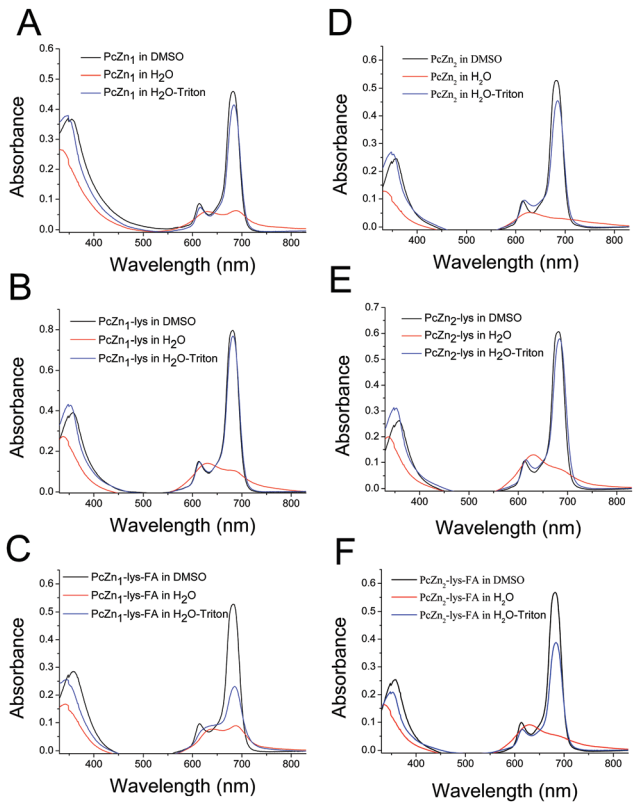

Fig. 3 Absorption spectra of $PcZn_1$ (a), $PcZn_1$-lys (b), $PcZn_1$-lys-FA (c), $PcZn_2$ (d) $PcZn_2$-lys (e) and $PcZn_2$-lys-FA (f) in DMSO (black), water (red) and water + Triton X-100 (blue) at 5 μM.

due to the decreased aggregation of these complexes. To test the influence of the presence of Triton X-100 on the fluorescence properties of these Pcs, the fluorescence emission spectra of $PcZn_1$-lys-FA were determined in the aqueous medium (concentration = 1.0×10^{-5} M) with the addition of varied concentrations of Triton X-100. As shown in Fig. 5, $PcZn_1$-lys-FA exhibited very low emission in water (approximately 1/100 of the intensity in DMSO), and the addition of Triton X-100 to the aqueous solution resulted in a significant increase in the fluorescence intensity. Addition of Triton X-100 to 1.25% increased the fluorescence intensity 20-fold, while an increase to 10% increased the fluorescence intensity 100-fold, with an intensity close to half of that in DMSO.

2.7. Fluorescence quantum yields, lifetimes and singlet oxygen quantum yields

Fluorescence quantum yield refers to the ratio of the number of photons emitted to the number of photons absorbed, and fluorescence lifetime refers to the average time that a molecule remains in its excited state before returning to its ground state. Upon excitation at 621 nm in DMSO, compounds **1–6** showed a fluorescence emission at 692–696 nm with a quantum yield of 0.12–0.14 and a fluorescence lifetime of approximately 3.0 ns. The quantum yields are low when compared to non-substituted ZnPc (quantum yield of 0.28 in DMSO). This is in accordance with the general observation that the lower the energy of the Q band, the smaller the quantum yield value.[28]

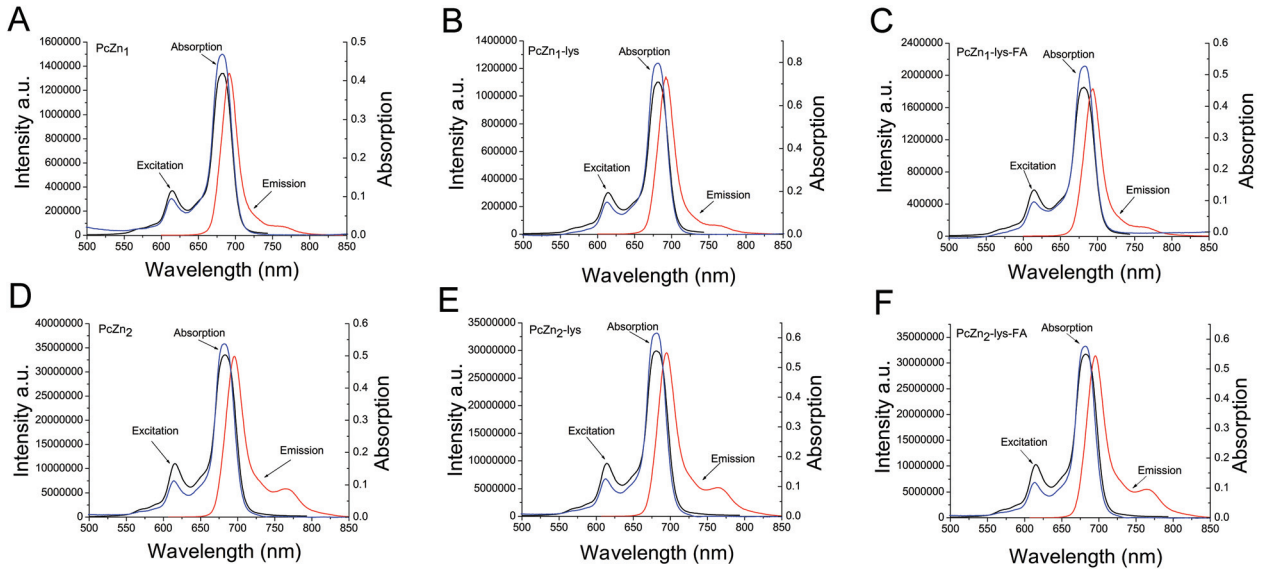

Fig. 4 Absorption, excitation and emission spectra of $PcZn_1$ (a), $PcZn_1$-lys (b), $PcZn_1$-lys-FA (c), $PcZn_2$ (d) $PcZn_2$-lys (e) and $PcZn_2$-lys-FA (f) in DMSO. Excitation wavelength: 615 nm.

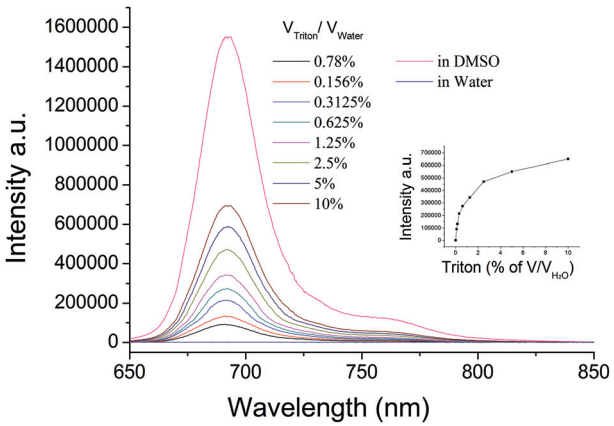

Fig. 5 Emission spectra of $PcZn_1$-lys-FA in water with varied concentrations of Triton X-100. Excitation wavelength: 615 nm.

A good photosensitizer must be very efficient in generating singlet oxygen. This is quantified by the parameter of the singlet oxygen quantum yield. The singlet oxygen quantum yields for Pcs **1–6** were determined using a chemical method by monitoring the disappearance of 1,3-diphenylisobenzofuran (DPBF) in DMSO with a UV–Vis spectrophotometer (shown in the ESI†). Non-substituted ZnPc was used as the reference. The results showed that all six of the synthesized Pcs have roughly the same singlet oxygen quantum yield values in the range 0.45–0.55, as shown in Table 2. These values are in a similar range when compared to the non-substituted ZnPc. The substituent ions have a very moderate influence on the singlet oxygen quantum yield. It should be noted that there was no decrease in the Q-band or formation of new bands during the singlet oxygen quantum yield determinations, indicating that the Pcs were not damaged by the generated singlet oxygen.

2.8. *In vitro* cellular uptake assays with confocal microscopy

Folate can act as the targeted ligand to enhance the specificity and cellular uptake of the cargo into folate receptor (FR)-overexpressing cancer cells. Therefore, the cellular uptake behavior of these folate-conjugated Pcs was investigated with human cervical cancer (HeLa) cells and murine embryonic fibroblast (NIH3T3) cells by analysis with fluorescence microscopy. After the cells were exposed to 50, 100 and 200 μM concentrations of $PcZn_1$-lys-FA or $PcZn_2$-lys-FA for 3 h, the Pc fluorescence could be detected and highly distributed inside the cells, indicating an efficient uptake of the Pcs by tumor cells (Fig. 6). Both compounds showed similar intracellular fluorescent patterns, with strong punctate fluorescence primarily distributed in the cytoplasm. These results are promising for the possible development of such conjugates for PDT. It should be noted that even these two Pcs, which are almost non-fluorescent in aqueous medium due to aggregation, show very strong fluorescence inside the cytoplasm. Cellular uptake can significantly increase the fluorescence intensity of Pcs, presumably due to monomerization of the aggregated dye species inside the cells. These compounds showed some selectivity for the FA receptor on the tumor cells. HeLa cells that have higher FA receptor expression levels took up more $PcZn_1$-lys-FA and $PcZn_2$-lys-FA than the NIH3T3 cells. However, the selectivity was not high and further improvements are needed to increase selectivity.

2.9. *In vivo* imaging of the distribution of Pcs in tumor-bearing mice

To examine the tumor-targeting capability of $PcZn_1$-lys-FA and $PcZn_2$-lys-FA *in vivo*, we prepared a xenograft tumor model by

Table 2 Photophysical and photochemical parameters of $PcZn_1$, $PcZn_1$-lys, $PcZn_1$-lys-FA, $PcZn_2$, $PcZn_2$-lys and $PcZn_2$-lys-FA in DMSO. Φ_F: fluorescence quantum yield, τ_F: fluorescence lifetimes, τ_0: natural radiative lifetime, κ_F: rate constants for fluorescence, Φ_Δ: singlet oxygen quantum yield. For ZnPcs, Φ_F = 0.18, Φ_Δ = 0.67

Compound	λ_{Ex}/nm	λ_{Em}/nm	Δ_{Stokes} (nm)	Φ_F	τ_F/ns	τ_0/ns	κ_F/s^{-1} ($\times 10^7$)	Φ_Δ
$PcZn_1$	682	692	10	0.13	3.33	25.6	3.9	0.50
$PcZn_1$-lys	684	692	10	0.12	3.02	25.2	4.0	0.50
$PcZn_1$-lys-FA	686	696	14	0.13	3.06	23.5	4.2	0.49
$PcZn_2$	683	696	15	0.14	3.73	26.6	3.8	0.53
$PcZn_2$-lys	682	695	13	0.13	3.19	24.5	4.1	0.56
$PcZn_2$-lys-FA	683	696	14	0.14	3.49	24.9	4.0	0.54

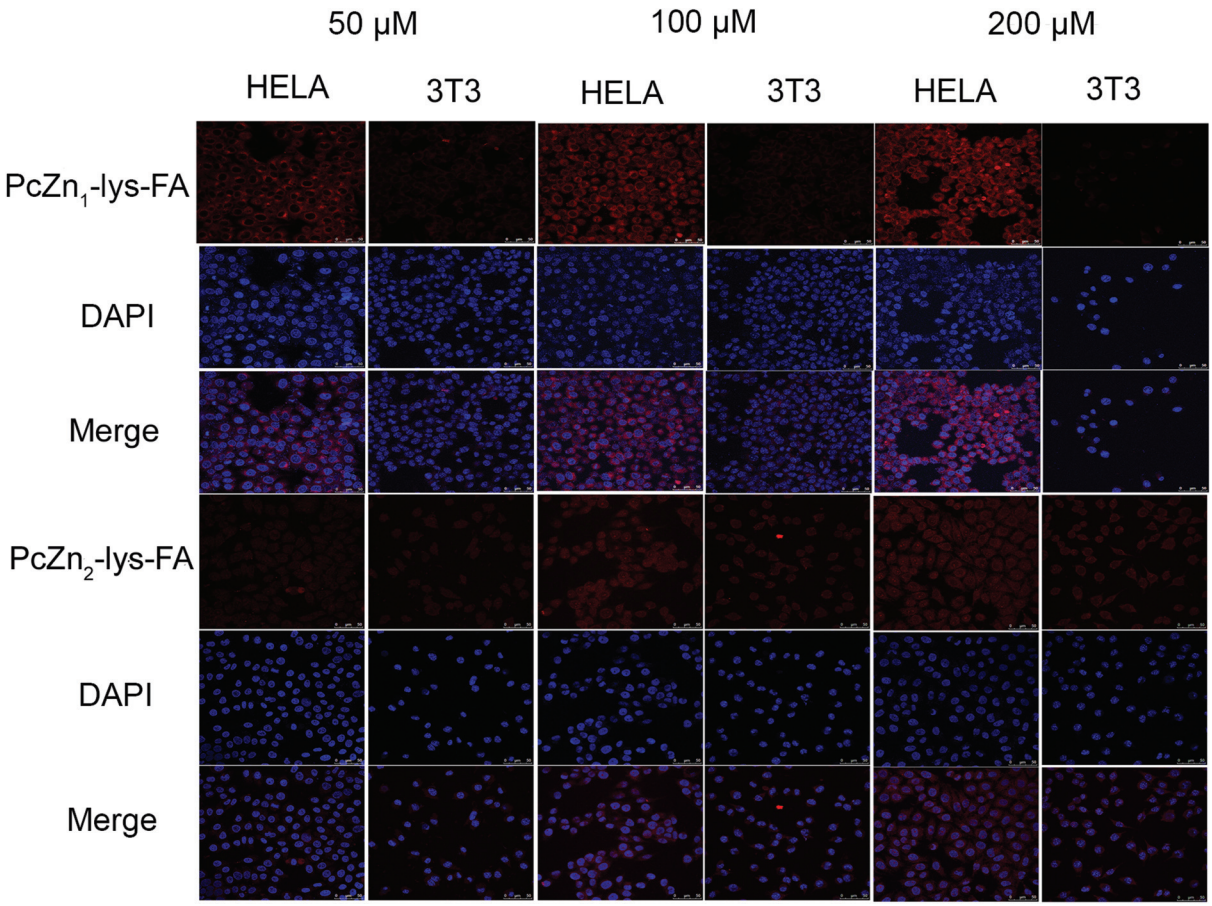

Fig. 6 Confocal images of cultured HeLa cells and NIH3T3 cells incubated with different concentrations of $PcZn_1$-lys-FA and $PcZn_2$-lys-FA (red). The nuclei of the cells were stained with DAPI (blue). Upper panels, incubated with $PcZn_1$-lys-FA; lower panels, incubated with $PcZn_2$-lys-FA.

subcutaneously inoculating mice with human epidermoid carcinoma (KB) cells (1.0×10^6 cells per mouse) in the dorsum. KB cells have high expression levels of the folate receptor. When tumors grew to approximately 50 mm^3 in volume, $PcZn_1$-lys-FA or $PcZn_2$-lys-FA (250 μg per mouse) was intra-venously injected into the mice *via* the tail vein. The fluorescence signal and intensity distribution of the Pcs were monitored continuously with an *in vivo* fluorescence imaging system (IVIS Lumina II, Xenogen, Alameda, CA, USA). As shown in Fig. 7A and C, $PcZn_1$-lys-FA injected into the mice showed strong fluorescence, visualized throughout the whole body of the mice in 5 min, but an intense fluorescence signal was primarily located in the liver, kidney and lung. After 3 h post-injection, the fluorescence signals began to decrease. However, the tumor-to-background ratios increased and accumulation in the tumor could be observed. Yet at 7 h post-injection, only very weak fluorescence signals could be detected and were primarily located in the tumor and lung. In contrast, the tumor distribution of $PcZn_2$-lys-FA was significantly different (as shown in Fig. 7B and D). In the tumor

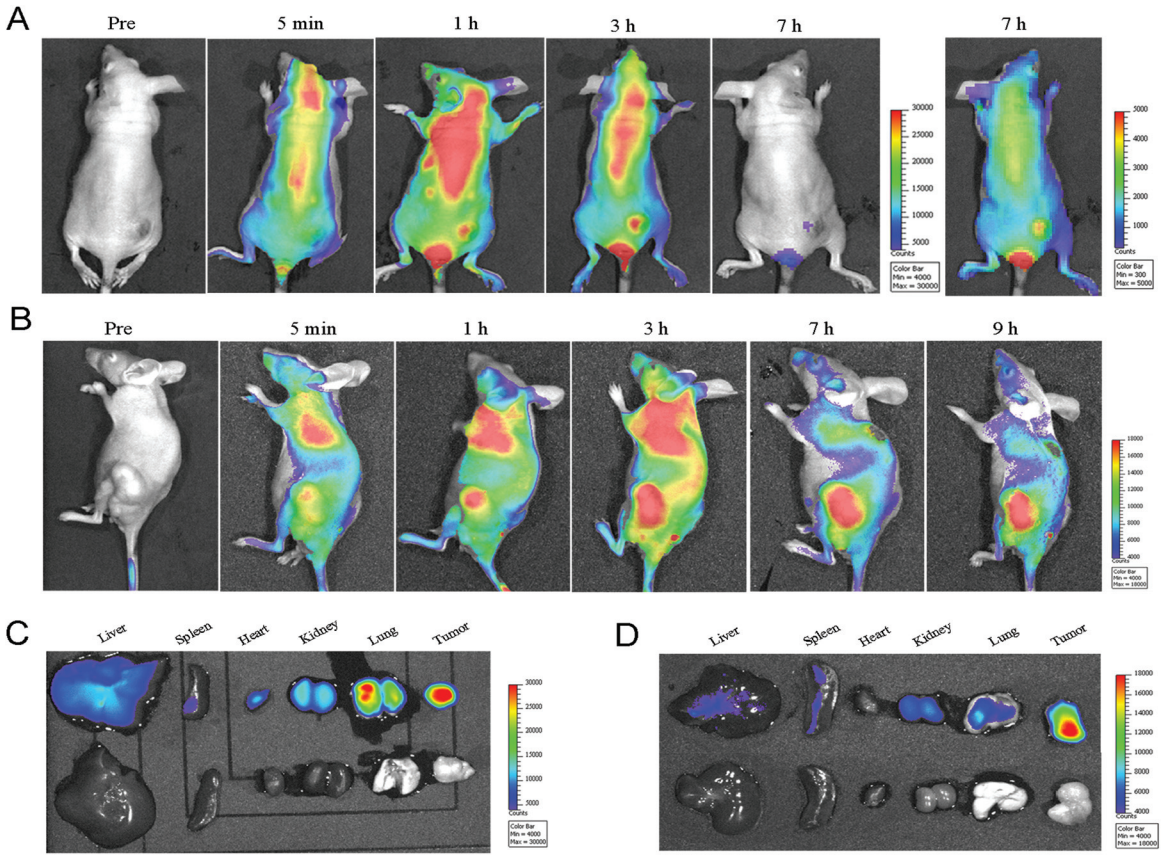

Fig. 7 Distribution of $PcZn_1$-lys-FA and $PcZn_2$-lys-FA (red) *in vivo* and in different organs. The BALB/c nude mice bearing KB human tumour xenografts at their spike were intravenously injected with $PcZn_1$-lys-FA and $PcZn_2$-lys-FA *via* the tail vein. (A) *In vivo* images of the mice treated with $PcZn_1$-lys-FA; (B) *In vivo* images of the mice treated with $PcZn_2$-lys-FA; (C) $PcZn_1$-lys-FA and (D) $PcZn_2$-lys-FA distribution in different organs: liver, spleen, heart, kidney, lung and tumor (from left to right).

region, the fluorescence intensity of $PcZn_2$-lys-FA was much stronger than that of $PcZn_1$-lys-FA. At 3 hours post injection, accumulation of the $PcZn_2$-lys-FA fluorescence signals in the tumor regions was already very strong. After 3 hours post injection, the fluorescence intensity in the tumors gradually increased, while the signal in other regions (including liver, spleen, heart, kidney and lung) were rapidly reduced, resulting in significantly increased tumor-to-background ratios. After 7 hours post injection, the signals were almost completely located in the tumor area; only negligible signals could be found in other tissues. These initial data provided strong evidence of high-specificity tumor targeting of $PcZn_2$-lys-FA with folate and tri-glycerol substitutions. The high hydrophilicity of glycerol moieties may have the ability to greatly reduce the non-specific affinity to normal tissues.

3. Conclusion

In conclusion, we developed a target-specific Pc based on a highly water-soluble folate-Pc conjugate. Here, we report the synthesis, basic photophysical properties, and *in vitro* and *in vivo* studies of these Pcs. $PcZn_2$-lys-FA can completely discriminate between healthy and tumor tissues in a subcutaneous xenograft tumor model, making this approach a promising therapeutic and diagnostic agent for the treatment of cancer. The ability to covalently conjugate many different ligands to Pcs means that this may be a highly flexible platform to synthesize Pcs for targeted PDT. The present investigations are preliminary studies in the search for more efficient photodynamic therapy agents based on Pcs.

4. Experimental section

4.1. Chemicals and materials

4-Nitrophthalonitrile, triethyleneglycol monomethylether, *S*-(+)-2,2-dimethyl-1,3-dioxolane-4-methanol and 4-hydroxybenzoic acid were purchased from Alfa Aesar (Tianjin, China). Triton X-100 and non-substituted ZnPc were purchased from Aldrich. 1,3-Diphenylisobenzofuran (DPBF) was purchased from J&K (Beijing, China). RPMI-1640 without folic acid was purchased from Sigma-Aldrich (St. Louis, MO, USA). Other chemical agents were purchased from Alfa Aesar (Tianjin, China).

4.2. Cells and animals

HeLa, NIH3T3 and KB cells were obtained from Saierbio (Tianjin, China). The cells were continuously cultured in folic acid-free RPMI 1640 medium supplemented with 10% fetal bovine serum (FBS) and 1% penicillin/streptomycin at 37 °C under a humidified atmosphere containing 5% CO_2. The final folic acid concentration (with FBS as the only source of folic acid) falls in the range of the physiological concentration of human serum. BALB/c nude mice (4–6 weeks of age) were purchased from Vital River Laboratory Animal Technology Co. Ltd (Beijing, China) and maintained in a germ-free environment with free access to food and water. All animal procedures were conducted under a protocol approved by the Institutional Animal Care and Use Committee of Nankai University (Tianjin, China).

4.3. Instruments

^{1}H and ^{13}C NMR spectra were recorded in DMSO-d_6 solutions on a Bruker AV400 400 MHz spectrometer. The mass spectra were recorded on Varian 7.0 T FTMS. Optical spectra in the UV-visible region were recorded with USA Cary 5000 using a 1 cm path length cuvette at room temperature. Fluorescence measurements were performed on a PTI QM/TM/NIR system (Photon Technology International, Birmingham, NJ, USA) equipped with a quartz cell (1 cm × 1 cm).

4.4. Synthesis experiments

Synthesis of phthalonitrile 9. To a solution of 4-nitrophthalonitrile (1.0 g, 5.78 mmol) in dry DMF (8 mL) were added triethyleneglycol monomethylether (1.42 g, 8.67 mmol) and finely ground K_2CO_3 (3.6 g, 26 mmol). The color of the solution turned from yellow to dark brown. The mixture was stirred at room temperature for 24 h before being poured into 350 mL of ice-water and left overnight. The resulting yellow precipitate was isolated by filtration and purified by column chromatography on silica gel with ethyl acetate–petroleum ether (1 : 1) as an eluting solvent to give a yellow solid (1.2 g) in 74% yield. ^{1}H NMR (400 MHz, $CDCl_3$) δ 7.70 (d, J = 8.8 Hz, 1H, Ar-H), 7.31 (d, J = 2.5 Hz, 1H, Ar-H), 7.22 (dd, J = 8.8, 2.6 Hz, 1H, Ar-H), 4.22 (dd, J = 5.2, 3.9 Hz, 2H, CH_2), 3.89 (dd, J = 5.2, 3.9 Hz, 2H, CH_2), 3.75–3.69 (m, 2H, CH_2), 3.69–3.61 (m, 4H, CH_2), 3.57–3.52 (m, 2H, CH_2), 3.38 (s, 3H, CH_2).

Synthesis of phthalonitrile 11. The solution of 4-nitrophthalonitrile (1.0 g, 5.78 mmol), *S*-(+)-2,2-dimethyl-1,3-dioxolane-4-methanol (764 μL, 5.78 mmol) and finely ground K_2CO_3 (3.6 g, 26 mmol) in dry DMF (8 mL) was stirred at 50 °C, checking for the completion (approximately 6 h) of the reaction by TLC (silica gel, hexane/ethyl acetate = 1/1). The reaction mixture was poured into ice water and left overnight. The resulting solid was filtered and purified by column chromatography (silica gel, hexane/ethyl acetate = 3/1) to yield 1.05 g of **11** (71%) as a white solid. ^{1}H NMR (400 MHz, $CDCl_3$) δ 7.73 (dd, J = 8.8, 4.2 Hz, 1H, Ar-H), 7.31 (d, J = 2.5 Hz, 1H, Ar-H), 7.23 (dd, J = 8.8, 2.6 Hz, 1H, Ar-H), 4.50 (dq, J = 11.0, 5.4 Hz, 1H), 4.18 (dt, J = 9.9, 4.9 Hz, 1H), 4.09 (qd, J = 9.7, 5.3 Hz, 2H), 3.89 (dt, J = 14.4, 7.2 Hz, 1H), 1.44 (s, 3H, CH_3), 1.40 (s, 3H, CH_3).

Synthesis of $PcZn_1$ (1). A solution of phthalonitrile **9** (145 mg, 0.5 mmol) and $Zn(OAc)_2{\cdot}2H_2O$ (60.4 mg, 0.25 mmol) in *n*-hexyl alcohol (2 mL) was heated to 120 °C to completely dissolve the salt before DBU (83.8 μL) was added. The mixture was stirred at 160 °C for 5 h. The product was solidified by pouring into 20 mL of petroleum ether and draining the solution. The green product was purified by silica gel chromatography using a dichloromethane : methanol mixture (20 : 1) as an eluent (94 mg, 62%). HRMS (ESI): calcd for $C_{60}H_{72}N_8NaO_{16}Zn$ $[M + Na]^+$ 1247.4250, found 1247.4251. ^{1}H NMR (400 MHz, DMSO-d_6) δ 8.81 (m, 4H, Ar-H), 8.34 (m, 4H, Ar-H), 7.58 (m, 4H, Ar-H), 4.63 (m, 8H, CH_2), 4.13 (m, 20H, CH_2 and CH_3), 3.91–3.81 (m, 8H, CH_2), 3.75 (m, J = 3.0 Hz, 8H, CH_2), 3.67 (m, J = 2.1 Hz, 8H, CH_2), 3.54 (m, 8H, CH_2). ^{13}C NMR (DMSO-d_6) overlapping signals at 159.85, 151.36, 139.69, 130.97, 122.99, 117.32, 105.25, 71.34, 69.71, 67.78, 58.00.

Synthesis of phthalocyanine 12. A mixture of phthalonitrile **11** (145.2 mg, 0.56 mmol), $Zn(OAc)_2{\cdot}2H_2O$ (41.2 mg, 0.188 mmol) in *n*-hexyl alcohol (2 mL) was heated to 120 °C for 10 min before DBU (76.5 μL) was added. The mixture was stirred at 160 °C for 5 h. The product was solidified by pouring into 20 mL of petroleum ether and draining the solution. The green product was purified by silica gel chromatography using PE : EA (2 : 3) as an eluent (107 mg, 70%). ^{1}H NMR (400 MHz, DMSO-d_6) δ 9.06 (s, 2H, Ar-H), 8.69 (s, 2H, Ar-H), 7.75 (d, J = 8.6 Hz, 4H, Ar-H), 7.46–7.25 (m, 4H, Ar-H), 4.77 (s, 2H), 4.61 (s, 4H), 4.42 (d, J = 26.4 Hz, 4H), 4.24 (s, 2H), 4.14 (s, 6H), 3.79 (s, 2H), 1.30 (dd, J = 34.7, 15.0 Hz, 24H, CH_3).

Synthesis of $PcZn_2$ (2). Compound **12** (100 mg, 0.09 mmol) was stirred in a solution of TFA : H_2O = 95 : 5 for 10 min. The reaction mixture was then evaporated to dryness under reduced pressure, and the dark blue powder was washed successively with ethyl acetate, hexane, dichloromethane and chloroform to yield **2** as a dark blue powder (78 mg, 93%). HRMS (ESI): calcd for $C_{44}H_{41}N_8O_{12}Zn$ $[M + H]^+$ 937.2130, found 937.2102. ^{1}H NMR (400 MHz, DMSO-d_6) δ 9.30 (m, 4H, Ar-H), 8.89 (m, 4H, Ar-H), 7.81 (m, 4H, Ar-H), 5.26 (m, 4H, CH_2), 4.94 (m, 4H, CH_2), 4.63 (m, 4H, CH), 4.51 (m, 4H, CH_2), 4.15 (m, 4H, CH_2), 3.73 (s, 8H, O-H). ^{13}C NMR (DMSO-d_6) overlapping signals at 160.45, 152.07, 139.65, 130.81, 123.15, 117.63, 105.56, 70.35, 63.00.

Synthesis of $PcZn_1$-lys (3). Phthalonitrile **9** (1.8 mmol) and $Zn(OAc)_2$ (0.6 mmol) were added to resin **13** (0.3 g, 0.0225 mmol) that was pre-swelled in anhydrous *n*-hexanol (3 mL) for 30 min. The mixture was heated to 120 °C for 10 min, and DBU (1.2 mmol, 163 μL) was added to the mixture. The reaction was carried out at 160 °C for 5 h. The mixture was solidified by pouring it into 30 mL of petroleum ether and draining the solution. The resin was washed with dichloromethane and methanol until a colorless filtrate was obtained. The resin was suspended into a solution of TFA/H_2O/triisopropylsilane (TIS) (95 : 2.5 : 2.5) and shaken for 1 h at room temperature. The filtrate was evaporated to dryness, and the crude mixture was purified by filtration through high

performance liquid chromatography (HPLC, LC-20AT, Shimadzu, Kyoto, Japan) to yield the product $PcZn_1$-lys as a blue solid (7.5 mg, 25% yield). HRMS (ESI): calcd for $C_{66}H_{75}N_{11}NaO_{15}Zn$ $[M + Na]^+$ 1348.4628, found 1348.4632. ^1H NMR (400 MHz, DMSO-d_6) δ 9.20 (m, 1H, NH), 9.04 (m, 3H, Ar-H), 8.71–8.51 (m, 3H, Ar-H), 8.18 (m, 2H, Ar-H), 7.69 (m, 4H, Ar-H), 7.58–7.47 (m, 2H, Ar-H), 7.11 (m, 2H, Ar-H), 4.67 (m, 6H, CH_2), 4.46 (m, 1H, CH), 4.10 (m, 6H, CH_2), 3.82 (m, 6H, CH_2), 3.71 (m, 6H, CH_2), 3.63 (m, J = 4.1 Hz, 6H, CH_2), 3.50 (m, J = 4.1 Hz, 6H, CH_2), 3.29–3.25 (m, 9H, CH_3), 2.82 (m, 2H, CH_2), 1.81 (m, 2H, NH_2), 1.59 (m, 2H, CH_2), 1.45 (m, 2H, CH_2), 1.24 (m, J = 11.2 Hz, 2H, CH_2).

Synthesis of $PcZn_2$-lys (4). Phthalonitrile **11** (1.8 mmol) and $Zn(OAc)_2$ (0.6 mmol) were added to resin **13** (0.3 g, 0.0225 mmol), which was pre-swelled in anhydrous *n*-hexanol (3 mL) for 30 min. The mixture was heated to 120 °C, and DBU (1.2 mmol, 163 μL) was added to the mixture. The reaction was conducted at 160 °C for 5 h. The mixture was solidified by pouring it into 30 mL of petroleum ether and draining the solution. The resin was washed with dichloromethane and methanol until a colorless filtrate was obtained. The resin was suspended in a solution of TFA/H_2O = 95/5 and shaken for 1 h at room temperature. The filtrate was evaporated to dryness, and the crude mixture was purified by filtration through high performance liquid chromatography (HPLC, LC-20AT, Shimadzu, Kyoto, Japan) to yield $PcZn_2$-lys as a blue solid (6.9 mg, 27% yield). HRMS (ESI): calcd for $C_{54}H_{51}N_{11}NaO_{12}Zn^+$ $[M + Na]^+$ 1132.2902, found 1132.2908. ^1H NMR (400 MHz, DMSO-d_6) δ 9.24 (m, 2H, Pc-Ar-H), 9.02–8.67 (m, 2H, Pc-Ar-H), 8.45 (m, 1H, Pc-Ar-H), 8.16 (m, 2H, Pc-Ar-H), 7.96 (m, 1H, Pc-Ar-H), 7.72 (m, 4H, 2Pc-Ar-H, 2Ar-H), 7.50 (m, 2H, Pc-Ar-H), 7.08 (m, 2H, Ar-H), 4.54 (m, 6H, CH_2), 4.14 (m, 3H, CH), 3.73 (m, 6H, CH_2), 2.81 (m, 2H, CH_2), 1.78 (m, 2H, CH_2), 1.59 (m, 2H, CH_2), 1.40 (s, 6H, O-H), 1.21 (m, J = 23.1 Hz, 2H, CH_2).

Synthesis of $PcZn_1$-lys-FA (5). The Mtt protecting group of resin **14** was deprotected in a solution of TFA/CH_2Cl_2/TIPS (1 : 98 : 1). Folic acid (0.11 mmol), HBTU (0.1 mmol) and DIEA (0.22 mmol) were dissolved in 5 mL of DMF/DMSO (1 : 1) and added to the resin. The mixture was agitated for 3 h in the dark and then washed with DMF/DMSO (1 : 1) (5 × 8.0 mL) to yield resin **16**. The resin **16** was suspended in a solution of TFA/H_2O/TIPS (95 : 2.5 : 2.5; 2 mL) and agitated for 1 h. The resin was removed by filtration. After removing the TFA of the filtrate in a vacuum, the residue was dissolved in DMSO and purified using high performance liquid chromatography (HPLC, LC-20AT, Shimadzu, Kyoto, Japan) to yield the product $PcZn_1$-lys-FA as a blue solid (3.1 mg, 7.9% yield). In the second strategy, phthalocyanine **3** (5.0 mg, 0.0037 mmol) was mixed with folic acid-NHS (3.0 mg, 0.0056 mmol) in DMSO and then triethylamine (2.0 μL) was added. The mixture was stirred in the dark for 8 h and purified with HPLC to yield the product $PcZn_1$-lys-FA as a blue solid (4.9 mg, 75%). HRMS (ESI): calcd for $C_{85}H_{92}N_{18}NaO_{20}Zn^+$ $[M + Na]^+$ 1771.5919, found 1771.5925. ^1H NMR (400 MHz, DMSO-d_6) δ 9.20 (m, 1H, NH), 9.01 (m, 3H, Pc-Ar-H), 8.62 (m, 4H, 3Pc-Ar-H, 1FA-Ar-H), 8.22 (m, 2H, Ar-H), 7.87 (m, 4H, 2Pc-Ar-H), 7.67 (m, 2H, 2FA-Ar-H), 7.51 (m, 2H, 2Pc-Ar-H), 7.09 (m, 2H, Ar-H), 6.64 (m, 2H, FA-Ar-H), 4.67–3.37 (m, 36H, CH_2), 3.10 (m, 9H, CH_3), 1.79–1.34 (m, 6H, CH_2).

Synthesis of $PcZn_2$-lys-FA (6). The Mtt protecting group of resin **15** was deprotected in a solution of TFA/CH_2Cl_2/TIPS (1 : 98 : 1). Folic acid (0.11 mmol), HBTU (0.1 mmol) and DIEA (0.22 mmol) were dissolved in 5 mL of DMF/DMSO (1 : 1) and added to the resin. The mixture was agitated for 3 h in the dark and then washed with DMF/DMSO (1 : 1) (5 × 8.0 mL) to yield resin **17**. The resin **17** was suspended in a cleavage cocktail of TFA/H_2O = 95 : 5 and purified using HPLC to yield the product $PcZn_2$-lys-FA as a blue solid (7.4 mg, 24% yield). In the second strategy, phthalocyanine **4** (4.2 mg, 0.0037 mmol) was mixed with folic acid-NHS (3.0 mg, 0.0056 mmol) in DMSO and then triethylamine (2.0 μL) was added. The mixture was stirred in the dark for 8 h and purified using HPLC to yield the product $PcZn_2$-lys-FA as a blue solid (4.5 mg, 80%). HRMS (ESI): calcd for $C_{73}H_{69}N_{18}O_{17}Zn^+$ $[M + H]^+$ 1533.4374, found 1533.4370. ^1H NMR (400 MHz, DMSO-d_6) δ 9.11 (m, 2H, Pc-Ar-H), 8.66–8.48 (m, 4H, 3Pc-Ar-H, 1FA-Ar-H), 8.19 (m, 3H, Pc-Ar-H), 7.88 (m, 4H, 2Pc-Ar-H, 2Ar-H), 7.66 (m, 4H, 2Pc-Ar-H, 2FA-Ar-H), 7.50 (m, 2H, Pc-Ar-H), 7.09 (m, 2H, Ar-H), 6.64 (m, 2H, FA-Ar-H), 4.54–3.10 (m, 27H, 16CH_2, 5CH, 6OH), 2.34–1.19 (m, 10H, CH_2).

4.5. Photophysical and photochemical properties

UV-Vis spectra. Optical spectra in the UV-Vis region were recorded in the wavelength range of 300–850 nm with a USA Cary 5000 using a 1 cm path length cuvette at room temperature.

Excitation and emission spectra. Fluorescence excitation and emission spectra were recorded in the wavelength range of 500–850 nm using 1 cm path length cuvettes at room temperature. The photomultiplier tube (PMT) voltage was set at 1074 V. The decayed curves of Pc emission at 692 nm were excited by the high resolution laser (N2 laser at 337 nm tuned by the laser dye PLD665) at 665 nm.

Quantum yield. The quantum yield (Φ_F) of Pcs in DMSO was determined on a PTI QM/TM/NIR system spectrometer under excitation of 665 nm, using a comparative method with the non-substituted ZnPc (Φ_F = 0.18 in DMSO)[29] as the reference,

$$\Phi_F = \Phi_{F(Std)} \frac{FA_{std}n^2}{F_{Std}An^2_{std}}$$

where F and F_{Std} are the areas under the fluorescence emission curves of the samples and the standard, respectively. A and A_{Std} are the respective absorbance of the samples and standard at the excitation wavelengths. n^2 and ${n_{std}}^2$ are the refractive indices of solvents used for the sample and standard, respectively. The absorbance of the solutions at the excitation wavelength ranged between 0.03 and 0.05.

Natural radiative lifetimes. Natural radiative lifetimes (τ_0) were determined using the PhotochemCAD program which uses the Strickler–Berg equation. The fluorescence lifetimes (τ_F) were evaluated using the equation: $\Phi_F = \frac{\tau_F}{\tau_0}$.

Singlet oxygen quantum yields. Singlet oxygen quantum yield (Φ_Δ) values were determined by the comparative method using 1,3-diphenylisobenzofuran (DPBF) as a singlet oxygen chemical quencher in DMSO with ZnPcs as references:

$$\Phi_\Delta = \Phi_\Delta^{Std} \frac{R I_{abs}^{Std}}{R^{Std} I_{abs}}$$

where Φ_Δ^{Std} is the singlet oxygen quantum yield for the standard ZnPc (Φ_Δ^{Std} = 0.67 in DMSO). R and R^{Std} are the DPBF photobleaching rates in the presence of respective samples and standards, respectively, and I_{abs} and I_{abs}^{Std} are the rates of light absorption by synthetic phthalocyanines and reference substances, respectively. The degradation of the solutions was monitored at 417 nm, and DPBF concentrations were lowered to ~2.5×10^{-5} mol L^{-1}. The light intensity of 6.0×10^{15} photons per s per cm^2 was used for Φ_Δ determinations.

4.6. *In vitro* cellular uptake assays

HeLa and NIH3T3 cells that were continuously cultured in folic acid-free RPMI 1640 medium supplemented with 10% FBS and 1% penicillin/streptomycin at 37 °C and 5% CO_2 were seeded into 24-well chambered coverglass (Lab-Tek, Nunc, USA) at a density of 5×10^4 cells per well (0.2 mL) 24 h before initiating the experiments. Two hours before the experiments, the medium was removed and replaced with 1.0 mL of fresh folic acid-deficient RPMI-1640. After incubation with a series of concentrations of $PcZn_1$-lys-FA or $PcZn_2$-lys-FA at 37 °C for 30 min, the cells were washed three times with phosphate buffer saline (PBS). The cells were then fixed with 4% formaldehyde for 10 min at room temperature and washed three times with PBS. Then, the cells were stained with 1 μg mL^{-1} DAPI for 3–5 min and washed three times with PBS. Confocal images were acquired using a Confocal Laser Scanning Microscope (TCS SP8, Leica, Wetzlar, Germany).

4.7. *In vivo* imaging

To set up the tumor model, Balb/c nude mice (8 weeks of age) were implanted with KB cells (2×10^6 cells per mouse in a volume of 100 μL) subcutaneously in the flank. When the tumor volumes reached approximately 50 mm^3 (approximately 10 days post-tumor inoculation), $PcZn_1$-lys-FA or $PcZn_2$-lys-FA was injected into the mice *via* the tail vein at a dose of 250 μg per mouse. Images were captured at 0, 5 min, 1 h, 4 h and 7 h after injection using the Xenogen *in vivo* imaging system with a Cy 5.5 filter (λ_{ex} = 615–665 nm, λ_{em} = 695–770 nm). The Xenogen images were obtained with the same settings (small binning value 2, exposure time 5 s, F/stop 1). The nude mice were sacrificed 7 or 9 h after injection. Then, the organs including liver, spleen, heart, lung, kidney and tumor were collected and analyzed by the Xenogen *in vivo* imaging system.

Acknowledgements

This work was supported by the Research Fund for the Doctoral Program of Higher Education of China (no. 20110031110019) and the National Natural Science Foundation of China (no. 31270926).

Notes and references

1 (*a*) H. Ali and J. E. van Lier, in *Handbook of Porphyrin Science*, ed. K. M. Kadish, K. M. Smith and R. Guilard, World Scientific, 2010, vol. 4, pp. 1–120; (*b*) A. P. Castano, P. Mroz and M. R. Hamblin, *Nat. Rev. Cancer*, 2006, **6**, 535; (*c*) D. E. Dolmans, D. Fukumura and R. K. Jain, *Nat. Rev. Cancer*, 2003, **3**, 380–387; (*d*) H. Ali and J. E. van Lier, *Chem. Rev.*, 1999, **99**, 2379.

2 (*a*) A. Juarranz, P. Jaen, F. Sanz-Rodriguez, J. Cuevas and S. Gonzalez, *Clin. Transl. Oncol.*, 2008, **10**, 148–154; (*b*) B. W. Henderson and T. J. Dougherty, *Photochem. Photobiol.*, 1992, **55**, 145–157.

3 S. B. Brown, E. A. Brown and I. Walker, *Lancet Oncol.*, 2004, **5**, 497.

4 (*a*) G. M. van Dam, G. Themelis, L. M. Crane, N. J. Harlaar, R. G. Pleijhuis, W. Kelder, A. Sarantopoulos, J. S. de Jong, H. J. Arts, A. G. van der Zee, J. Bart, P. S. Low and V. Ntziachristos, *Nat. Med.*, 2011, **17**, 10; (*b*) Q. T. Nguyen, E. S. Olson, T. A. Aguilera, T. Jiang, M. Scadeng and L. G. Ellies, *Proc. Natl. Acad. Sci. U. S. A.*, 2010, **107**, 4317–4322; (*c*) H. Kobayashi, M. Ogawa, R. Alford, P. L. Choyke and Y. Urano, *Chem. Rev.*, 2010, **110**, 2620–2640.

5 (*a*) L. B. Josefsen and R. W. Boyle, *Theranostics*, 2012, **2**, 916–966; (*b*) J. P. Celli, B. Q. Spring, I. Rizvi, C. L. Evans, K. S. Samkoe, S. Verma, B. W. Pogue and T. Hasan, *Chem. Rev.*, 2010, **110**, 2795–2838.

6 P. Agostinis, K. Berg, K. A. Cengel, T. H. Foster, A. W. Girotti, S. O. Gollnick, S. M. Hahn, M. R. Hamblin, A. Juzeniene, D. Kessel, M. Korbelik, J. Moan, P. Mroz, D. Nowis, J. Piette, B. C. Wilson and J. Golab, *CA-Cancer J. Clin.*, 2011, **61**, 250–281.

7 (*a*) S. L. Gibbs, *Quant. Imaging Med. Surg.*, 2012, **2**, 177–187; (*b*) N. M. Idris, M. K. Gnanasammandhan, J. Zhang, P. C. Ho, R. Mahendran and Y. Zhang, *Nat. Med.*, 2012, **18**, 1580–1585; (*c*) M. Ethirajan, Y. Chen, P. Joshi and R. K. Pandey, *Chem. Soc. Rev.*, 2011, **40**, 340–362; (*d*) S. Luo, E. Zhang, Y. Su, T. Cheng and C. Shi, *Biomaterials*, 2011, **32**, 7127–7138; (*e*) H. Kobayashi, M. Ogawa, R. Alford, P. L. Choyke and Y. Urano, *Chem. Rev.*, 2010, **110**, 2620–2640.

8 M. Ethirajan, Y. Chen, P. Joshi and R. K. Pandey, *Chem. Soc. Rev.*, 2011, **40**, 340–362.

9 (*a*) J.-P. Taquet, C. Frochot, V. Manneville and M. Barberi-Heyob, *Curr. Med. Chem.*, 2007, **14**, 1673–1687; (*b*) T. Nyokong, *Coord. Chem. Rev.*, 2007, **251**, 1707; (*c*) R. Hudson and R. W. J. Boyle, *J. Porphyrins Phthalocyanines*, 2004, **8**, 954–975.

10 J. D. Spikes, *Photochem. Photobiol.*, 1986, **43**, 691–699.

11 V. T. Verdree, S. Pakhomov, G. Su, M. W. Allen, A. C. Countryman, R. P. Hammer and S. A. Soper, *J. Fluoresc.*, 2007, **17**, 547–563.

12 F. Dumoulin, M. Durmus, V. Ahsen and T. Nyokong, *Coord. Chem. Rev.*, 2010, **254**, 2792–2847.
13 K. E. Sekhosana and T. Nyokong, *Opt. Mater.*, 2014, **37**, 139–146.
14 (*a*) I. Laville, S. Pigaglio, J. C. Blais, F. Doz, B. Loock, P. Maillard, D. S. Grierson and J. Blais, *J. Med. Chem.*, 2006, **49**, 2558–2567; (*b*) S. Ballut, D. Naud-Martin, B. Loock and P. Maillard, *J. Org. Chem.*, 2011, **76**, 2010–2028; (*c*) F. Hammerer, G. Garcia, S. Chen, F. Poyer, S. Achelle, C. Fiorini-Debuisschert, M. P. Teulade-Fichou and P. Maillard, *J. Org. Chem.*, 2014, **79**, 1406–1417; (*d*) J. Gravier, R. Schneider, C. Frochot, T. Bastogne, F. Schmitt, J. Didelon, F. Guillemin and M. Barberi-Heyob, *J. Med. Chem.*, 2008, **51**, 3867–3877; (*e*) V. Sarrazy, G. Garcia, J. P. MBakidi, C. L. Morvan, G. Bégaud-Grimaud, R. Granet, V. Sol and P. Krausz, *J. Photochem. Photobiol., B*, 2011, **103**, 201–206; (*f*) G. Garcia, V. Sol, F. Lamarche, R. Granet, M. Guilloton, Y. Champavier and P. Krausz, *Bioorg. Med. Chem. Lett.*, 2006, **16**, 3188–3192.
15 (*a*) M. Kuruppuarachchi, H. Savoie, A. Lowry, C. Alonso and R. W. Boyle, *Mol. Pharmaceutics*, 2011, **8**, 920–931; (*b*) F. C. Rossetti, L. B. Lopes, A. R. H. Carollo, J. A. Thomazini, A. C. Tedesco, M. Vitória and L. B. Bentley, *J. Controlled Release*, 2011, **155**, 400–408; (*c*) E. Ricci-Júnior and J. M. Marchetti, *Int. J. Pharm.*, 2006, **310**, 187–195; (*d*) P. Jacques and A. M. Braun, *Helv. Chim. Acta*, 1981, **64**, 1800.
16 C. Dubuc, R. Langlois, F. Benard, N. Cauchon, K. Klarskov, P. Tone and J. E. van Lier, *Bioorg. Med. Chem. Lett.*, 2008, **18**, 2424–2427.
17 (*a*) N. Masilela, M. Idowu and T. Nyokong, *J. Photochem. Photobiol., A*, 2009, **201**, 91; (*b*) W. Liu, T. J. Jensen, F. R. Fronczek, R. P. Hammer, K. M. Smith and M. G. H. Vicente, *J. Med. Chem.*, 2005, **48**, 1033.
18 J. Alzeer, B. R. Vummidi, P. J. C. Roth and N. W. Luedtke, *Angew. Chem., Int. Ed.*, 2009, **48**, 9362.
19 (*a*) H. Li, T. J. Jensen, F. R. Fronczek and M. G. H. Vicente, *J. Med. Chem.*, 2008, **51**, 502; (*b*) S. Makhseed, M. Machacek, W. Alfadly, A. Tuhl, M. Vinodh, T. Simunek, V. Novakova, P. Kubat, E. Rudolf and P. Zimcik, *Chem. Commun.*, 2013, **49**, 11149–11151.
20 A. Pashkovskaya, E. Kotova, Y. Zorlu, F. Dumoulin, V. Ahsen, I. Agapov and Y. Antonenko, *Langmuir*, 2010, **26**, 5726.
21 Y. Zorlu, M. A. Ermeydan, F. Dumoulin, V. Ahsen, H. Savoie and R. W. Boyle, *Photochem. Photobiol. Sci.*, 2009, **8**, 312.
22 (*a*) R. A. Petros and J. M. Simone, *Nat. Rev. Drug Discovery*, 2010, **9**, 615–627; (*b*) M. A. C. Stuart, W. T. S. Huck, J. Genzer, M. Muller, C. Ober, M. Stamm, G. B. Sukhorukov, I. Szleifer, V. V. Tsukruk, M. Urban, F. Winnik, S. Zauscher, I. Luzinov and S. Minko, *Nat. Mater.*, 2010, **9**, 101–113.
23 (*a*) M. Mitsunaga, M. Ogawa, N. Kosaka, L. T. Rosenblum, P. L. Choyke and H. Kobayashi, *Nat. Med.*, 2011, **17**(12), 1685–1691; (*b*) C. Alonso and R. W. Boyle, in *Handbook of Porphyrin Science*, ed. K. M. Kadish, K. M. Smith and R. Guilard, World Scientific, 2010, vol. 4, pp. 121–190; (*c*) C. Alonso, A. Palumbo, A. J. Bullous, F. Pretto, D. Neri and R. W. Boyle, *Bioconjugate Chem.*, 2010, **21**, 302–313.
24 E. Ranyuk, N. Cauchon, K. Klarskov, B. Guérin and J. E. van Lier, *J. Med. Chem.*, 2013, **56**, 1520–1534.
25 A. Wang, L. Long and C. Zhang, *Tetrahedron*, 2012, **68**, 2433–2451.
26 (*a*) S. S. Erdem, I. V. Nesterova, S. A. Soper and R. P. Hammer, *J. Org. Chem.*, 2009, **74**, 9280–9286; (*b*) S. S. Erdem, I. V. Nesterova, S. A. Soper and R. P. Hammer, *J. Org. Chem.*, 2008, **73**, 5003–5007.
27 For the conjugation of folic acid with photosensitizers, see: (*a*) B. S. Wang, J. Wang and J. Y. Chen, *J. Mater. Chem. B*, 2014, **2**, 1594–1602. For the application of folic acid in drug delivery and imaging, see: (*b*) W. Xia and P. S. Low, *J. Med. Chem.*, 2010, **53**, 6811–6824; (*c*) D. K. Armstrong, A. Bicher, R. L. Coleman, D. G. Gibbon, D. Glenn, L. Old, N. N. Senzer, A. Schneeweiss, R. H. Verheijen, A. J. White and S. Weil, *J. Clin. Oncol.*, 2008, **26**, 5500; (*d*) L. C. Hartmann, G. L. Keeney, W. L. Lingle, T. J. Christianson, B. Varghese, D. Hillman, A. L. Oberg and P. S. Low, *Int. J. Cancer*, 2007, **121**, 938–942.
28 N. Kobayashi, H. Ogata, N. Nonaka and E. A. Luk'yanets, *Chem. – Eur. J.*, 2003, **9**, 5123–5134.
29 P. Jacques and A. M. Braun, *Helv. Chim. Acta*, 1981, **64**, 1800–1806.

